PCCP
Physical Chemistry Chemical Physics

This article can be cited before page numbers have been issued, to do this please use: I. Kulszewicz-Bajer, M. Zagorska, M. Banasiewicz, P. A. Guka, P. Toman, B. Kozankiewicz, G. Wiosna-Sayga and A. Pron, *Phys. Chem. Chem. Phys.*, 2020, DOI: 10.1039/D0CP00521E.

View Article Online
DOI: 10.1039/D0CP00521E

Effect of substituent position on electrochemical, optical and structural properties of donor-acceptor type acridone derivatives

Received 00th January 20xx,
Accepted 00th January 20xx

DOI: 10.1039/x0xx00000x

Irena Kulszewicz-Bajer,*[a] Malgorzata Zagorska,*[a] Marzena Banasiewicz,[b] Piotr A. Guńka,[a] Petr Toman,[c] Boleslaw Kozankiewicz,[b] Gabriela Wiosna-Salyga[d] and Adam Pron*[a]

Three new donor-acceptor (D-A) compounds were synthesized - positional isomers of phenoxazine-substituted acridone, namely 1-phenoxazine-*N*-hexylacridone (***o*-A**), 2-phenoxazine-*N*-hexylacridone (***m*-A**) and 3-phenoxazine-*N*-hexylacridone (***p*-A**). The synthesized compounds showed interesting, isomerism-dependent electrochemistry. Their oxidation was reversible and its potential (given *vs* Fc/Fc$^+$) changed from 0.21 V for ***o*-A** to 0.36 V for ***p*-A.** To the contrary, their reduction was irreversible, isomerism-independent and occurred at rather low potentials (*ca.*-2.25 to -2.28 V). The electrochemical results led to the following values of the ionization potentials (IPs) and electron affinities (EAs): 5.03 eV and -2.14 eV, 5.15 eV and -2.20 eV, 5.20 eV and -2.28 eV for ***o*-A, *m*-A** and ***p*-A**, respectively. The experimentally obtained values were in a very good agreement with those predicted by DFT calculations. All three isomers readily formed single crystals suitable for their structure determination. ***o*-A** and ***p*-A** crystallized in $P\bar{1}$ and $P2_1/n$ space groups, respectively, with one molecule per asymmetric unit, while ***m*-A** crystallized in the $P2_1/c$ space group with two molecules in the asymmetric unit accompanied by disordered solvent molecules. The UV-vis spectra of the studied compounds were isomerism and solvent independent, yielding absorption maxima in the vicinity of 400 nm. Their photoluminescence spectra, in turn, strongly depended on isomerism and the used solvent showing smaller Stokes shifts for the emission bands registered in toluene as compared to the corresponding bands measured in dichloromethane. The photoluminescence quantum yields (ϕ) were systematically higher for toluene solutions reaching the highest value of 20% for ***p*-A**. For all three isomers studied, stationary and time-resolved spectroscopic investigations carried in toluene at different temperatures revealed spectral features indicating a contribution of thermally-activated delayed fluorescence (TADF) to the observed spectroscopic behaviour. The measured photoluminescence quantum yields (ϕ) were higher for solid state films of pure compounds and for their dispersions in solid matrices (zeonex) than those recorded for toluene and dichloromethane solutions of the studied phenoxazine-*N*-hexylacridone isomers. The obtained experimental spectroscopic and structural data were confronted with theoretical predictions based on DFT calculations.

.

Introduction

Low and high molecular mass donor-acceptor compounds of DA and DAD type deserve a special interest because they offer interesting electrochemical and optical properties, mainly associated with their high electron affinity (EA) and relatively low ionization potential (IP) which give rise, among others, to their low band gaps.[1-4] As a result they are very well suited for the use as active components of organic solar cells,[5,6] one component ambipolar organic field effect transistors[7-9] and OLEDs emitting visible or near infrared radiation, including those which exploit the temperature activated delayed fluorescence (TADF) effect where a small energy gap between the singlet and triplet states, $\Delta E_{ST} < 0.1$ eV is required.[10-12] Electrochemical applications of DA compounds involve mainly the elaboration of new electrochromic devices[13,14] and electrochemical supercapacitors based on pseudocapacitance phenomena.[15,16]

All physical and chemical properties of DA and DAD molecules are very sensitive to isomerism since the molecules geometries and by consequence their electronic structures strongly depend on the way the D substituent is being attached to the A core. The substitution mode can have strong effects on the oxidation/reduction potentials of DA and DAD compounds, their electrochemical reversibility, the absorption and emission spectra and other properties. 2D and 3D supramolecular organizations are also affected by positional and geometrical isomerism.[17,18]

---

[a] *Faculty of Chemistry, Warsaw University of Technology, Noakowskiego 3, 00-664 Warsaw, Poland.*
[b] *Institute of Physics, Polish Academy of Sciences, Al. Lotnikow 32/44, 02-668 Warsaw, Poland.*
[c] *Institute of Macromolecular Chemistry, Academy of Sciences of the Czech Republic, Heyrovsky Sq. 2, 162 06 Prague 6, Czech Republic.*
[d] *Department of Molecular Physics, Technical University of Lodz, Zeromskiego 116, 90-924 Lodz, Poland.*

† Electronic Supplementary Information (ESI) available: [synthetic details, characterization of compounds, electrochemical, spectroscopic, X-ray diffraction studies, calculation details]. See DOI: 10.1039/x0xx00000x

View Article Online
DOI: 10.1039/D0CP00521E

Acridone seems to be a very promising acceptor in the development of electrochemically and optically active DA and DAD compounds. It is not a strong acceptor but it shows excellent chemical and thermal stabilities. Surprisingly the reports on acridone-based electroactive and luminescent compounds are rather scarce. Acridone derivatives were used in organic electronics as hole transporting materials[19] and as luminophores whose emission colors depended on the nature of D substituents.[20,21] In particular, it was demonstrated that diarylamine-disubstituted *N*-methylacridone, namely 2,7-bis(anisylamino)-*N*-methylacridone, showed emission peaked at 527 nm,[22] whereas carbazole disubstituted *N*-hexylacridone ((2,7-bis(carbazole)-*N*-hexylacridone) revealed an emission band at 469 nm.[23] Taking into account the above described sensitivity of DA compounds to positional isomerism we synthesized three new acridone derivatives in which a strong donor (phenoxazine) was attached to this relatively weak acceptor (*N*-hexylacridone) at three different positions: *ortho, meta* and *para*, respectively. We carried out a detailed characterization of these compounds combining electrochemical, absorption and emission spectroscopic experimental data with DFT calculations. We also determined their crystal structures. Finally, for comparative reasons we synthesized an acridone derivative disubstituted with phenoxazine (2,7-bis(phenoxazine)-*N*-hexylacridone).

Experimental

Synthesis

Detailed descriptions of the preparation procedures, crystal structure determination together with NMR data and elemental analysis can be found in *Electronic supplementary information (ESI)*.

Characterization

UV-vis absorption spectra of the synthesized compounds dissolved in dichloromethane and toluene were recorded on a Perkin-Elmer Lambda 35 spectrophotometer. Emission spectra and fluorescence lifetimes at room temperature were collected on a Horiba Fluorolog 3 fluorimeter. Excitation for fluorescence lifetimes measurements was provided by Delta Diode 336 nm. The solid state emission spectra were recorded on a FLS980 (Edinburgh Instruments) spectrometer. Absolute quantum yields of thin films were measured in an integrating sphere, coated inside with BENFLEC®, provided by Edinburgh Instruments. Optical, emission studies at low temperatures were performed using a standard synchronous-chopper phosphorimetry technique.[10] The solution of acridone derivative in liquid toluene was poured into a small cylinder-shaped fused silica cuvette and quickly cooled in liquid nitrogen (77 K) in order to prevent aggregation. Next, a sample holder with the frozen sample was quickly inserted into a cold cryostat which temperature was stabilized between 5 and 150 K. Sample was illuminated with the 405 nm line from a diode laser and the emission, dispersed with a McPherson 207 monochromator, was detected with an EMI9659 photomultiplier (operating in the photon counting mode). Phosphorescence decays were accumulated with a Stanford Research SR-430 Multichannel Scaler. Electrochemical measurements (CV and DPV) were performed using Autolab potentiostat (Eco Chemie). 1x10^{-3}M solution of studied compounds in 0.1M Bu_4NBF_4/CH_2Cl_2 electrolyte was placed in a three electrode, one-compartment cell with platinum working and counter electrodes and an Ag/Ag^+ reference.

Quantum chemical calculations

Quantum chemical calculations were carried out with the goal to theoretically support the obtained electrochemical and spectroscopic data.

The ground state molecular conformations of the neutral molecules of the studied derivatives and their cation-radicals and anion-radicals were optimized using hybrid Hartree–Fock/Density Functional Theory (DFT) method B3LYP.[24,25] In order to account for intramolecular dispersion forces between conjugated molecular moieties B3LYP method was combined with the Grimme empirical dispersion correction with the Becke-Johnson damping (GD3BJ).[26] The 6-311++G(d,p) basis set was used. The dispersion-corrected DFT methods usually provides reliable ground-state molecular conformations and other properties at moderate computational costs. Furthermore, their application to the open-shell systems (ion-radicals) does not suffer from high spin contamination, which is common for wave-function based methods. They have been successfully used for the conformation study of many different conjugated systems.[27-29] Molecular conformations were calculated for both the isolated molecules (in vacuum) and molecules in a solution. Solvation effects were described by means of the polarizable continuum model (PCM) using the integral equation formalism variant.[30] The obtained equilibrium structures were checked by the normal mode analysis (no imaginary frequency was found). Vertical and adiabatic ionization potentials and electron affinities were evaluated from differences of the total energies of the neutral molecules and respective ion-radicals (so-called ΔSCF method). The vertical absorption spectra in toluene and dichloromethane solution were computed by the time dependent version (TD-)[31-33] of the PCM-B3LYP-GD3BJ/6-311++G(d,p) method at the ground-state molecular geometries. All calculations of the electrochemical properties and absorption spectra were performed using Gaussian 16 program package.[34]

In view of the importance of theoretical calculations in the elucidation of TADF phenomena we have included into Electronic Supplementary Information details concerning theoretical background of the thermally activated delayed fluorescence modelling.

Results and discussion

Synthesis

View Article Online
DOI: 10.1039/D0CP00521E

The studied compounds *i.e.* (1-phenoxazine-*N*-hexylacridone, 2-phenoxazine-*N*-hexylacridone, 3-phenoxazine-*N*-hexylacridone and 2,7-bis(phenoxazine)-N-hexylacridone) are depicted in Chart 1. In the subsequent text they will be abbreviated as: ***o*-A**, ***m*-A**, ***p*-A** and **di-*m*-A**.

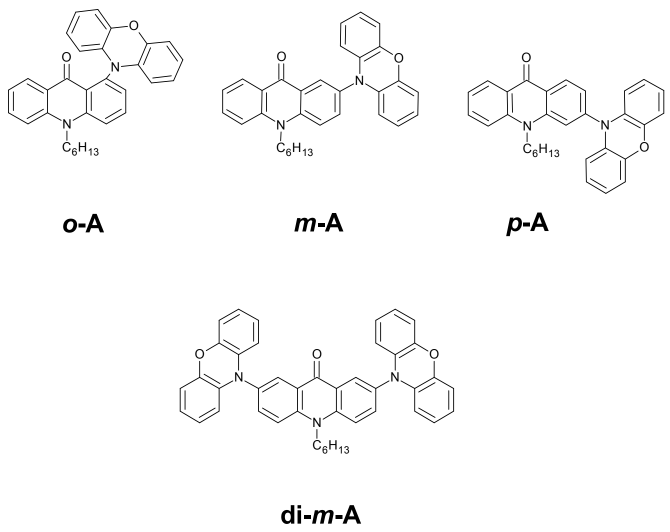

Chart 1. Structural formulae of the studied acridone derivatives.

The synthetic pathway leading to the studied derivatives is depicted in *Scheme 1*. *N*-3-bromophenyl-2-anthranilic acid **1** was prepared following a modification of the method described in.[35] Its cyclization in the presence of polyphosphoric acid resulted in a mixture of 1-bromo- and 3-bromoacridones. Both isomers were directly alkylated with n-hexyl bromide yielding, after chromatographic separation, *N*-hexyl-1-bromoacridone **2a** and *N*-hexyl-3-bromoacridone **2b** in a molar ratio 3:2 (the overall yield was 73%). *N*-hexyl-2-bromoacridone **2c** was obtained by bromination of *N*-hexylacridone with bromine in acetic acid/sodium acetate medium (47% yield). Buchwald-Hartwig amination coupling of these bromoderivatives, using phenoxazine and Pddba$_2$/t-Bu$_3$P catalyst, yielded the desired products: ***o*-A** (53% yield); ***p*-A** (87% yield) and ***m*-A** (92% yield). Disubstituted acridone derivative was obtained *via* bromination of *N*-hexylacridone core at 2,7 positions (in a process similar to monobromination mentioned above) followed by the amination with phenoxazine (82% yield).

Detailed description of all synthetic procedures can be found in *ESI.*

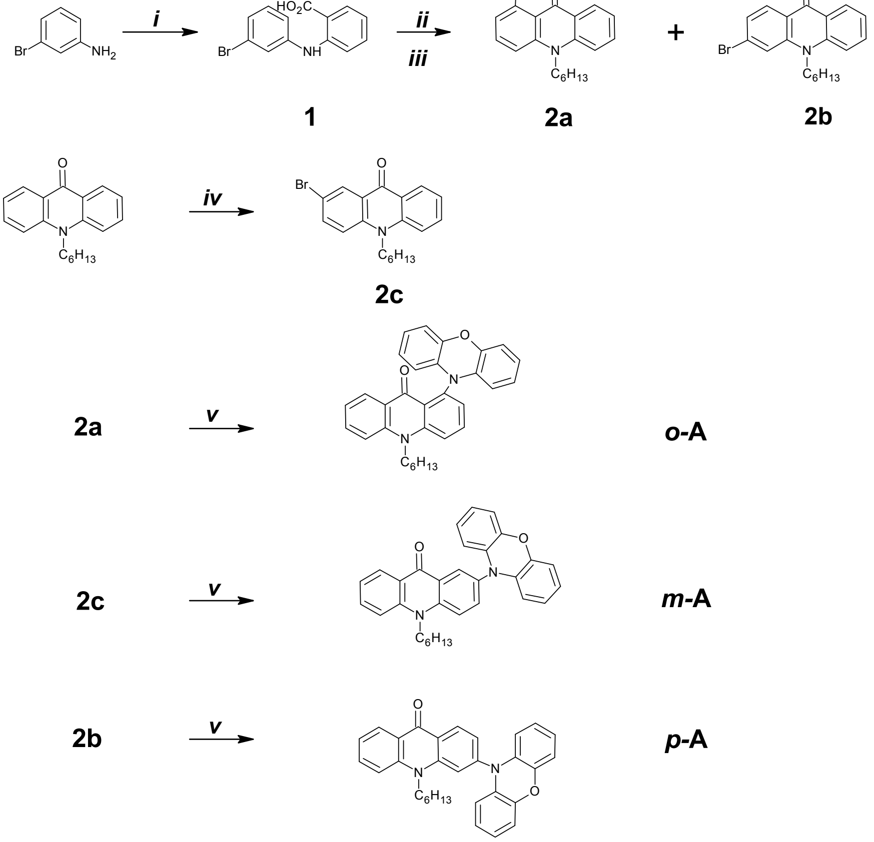

Scheme 1. Synthetic routes to phenoxazine-substituted *N*‑hexylacridones i) 2-bromobenzoic acid, K$_2$CO$_3$, Cu/Cu$_2$O, 2-ethoxyethanol, 130 °C, ii) polyphosphoric acid, 170 °C, iii) 1-bromohexane, Cs$_2$CO$_3$, NMP, 100 °C, iv) Br$_2$, NaOAc, acetic acid, 130 °C, v) phenoxazine, Pddba$_2$, *t*-Bu$_3$P, *t*-BuONa, toluene, 90 °C.

View Article Online
DOI: 10.1039/D0CP00521E

Electrochemical investigations

Cyclic voltammetry investigations constitute an important part of the characterization of new electroactive compounds since they not only provide general information on their redox properties but also allow for the calculations of their ionization potential (IP) and electron affinity (EA) – two parameters of predictive character as far as applications of these new compounds in electronics, optoelectronics and electrochromism are envisioned.

A representative CV voltammogram of ***o*-A** is shown in Figure 1 and compared with the corresponding data recorded for *N*-hexylphenoxazine and *N*-hexylacridone *i.e.* compounds mimicking, respectively, the donor and acceptor segments of the studied DA compounds. CV and differential pulse (DP) voltammograms of ***p*-A**, ***m*-A** and **di-*m*-A** can be found in *ESI* (Figure S1 and S2). All electrochemical data are collected in Table 1. There are some common features in the electrochemical behavior of the studied compounds. First, based on the oxidation potentials values it can be postulated that the three derivatives undergo reversible oxidation of their phenoxazine part to a radical cation. The potential of this oxidation, which is strongly dependent on the substitution position, decreases in a series ***p*-A**>***m*-A**>***o*-A** (see Figure 2), in the latter case it is even slightly lower than the corresponding potential of *N*-hexylphenoxazine. Second, the reduction of the *N*-hexylacridone to a radical anion is irreversible and much less dependent on the substitution position. The irreversibility of the reduction process is undoubtedly associated with low stability of radical anions electrochemically generated at very low potentials. It should be noted that in all three cases the reduction potential, although low, is higher than that of *N*-hexylacridone. The introduction of the second phenoxazine substituent to yield symmetrical DAD compound (**di-*m*-A** derivative) only slightly increases the reduction potential by 60 mV (see Table 1).

For the calculations of IP and EA, the potentials of the reduction and oxidation peaks onsets were taken because the formal redox potential could not be determined for the reduction process due to its irreversibility. The lowest "electrochemical" band gap was found for ***o*-A**, mainly because of its significantly lower oxidation potential as compared to the other compounds studied. The addition of the second substituent of electro-donating properties lowered the band gap by only 60 meV (compare ***m*-A** and **di-*m*-A**). These intuitively rather unexpected results, *ie.* the lowest Eg for ***o*-A** and the highest Eg for ***p*-A**, required a theoretical support. For these reasons detailed DFT calculations were performed.

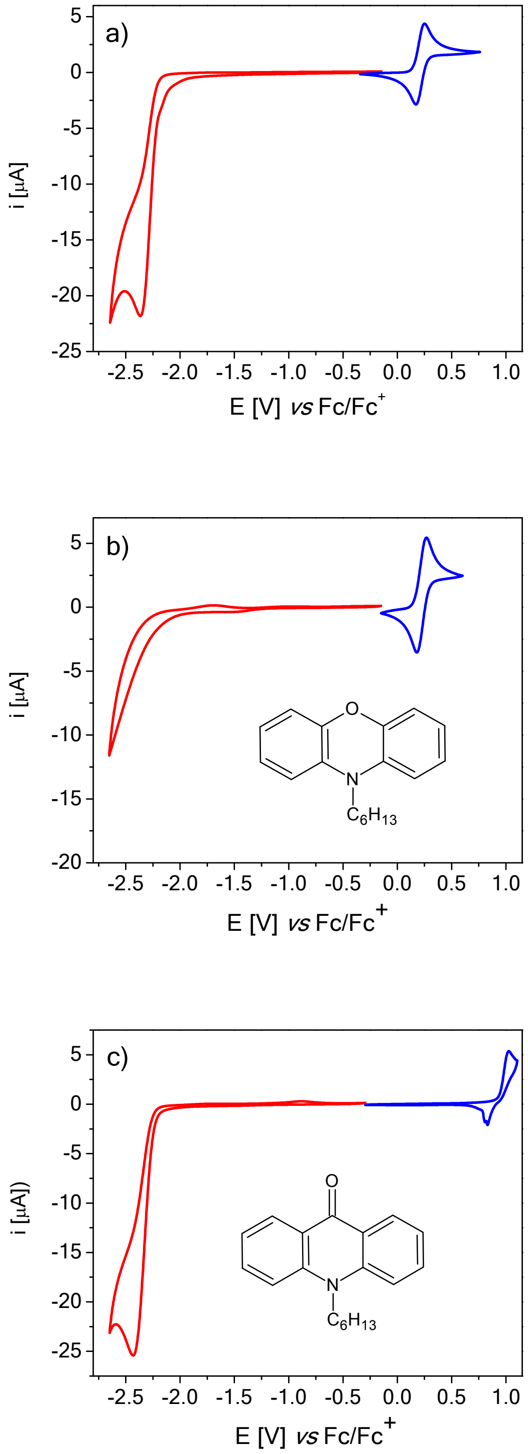

Fig. 1. Cyclic voltammograms registered for: a) ***o*-A**; b) *N*-hexylphenoxazine c) *N*-hexylacridone. Electrolyte: 0.1M Bu_4NBF_4/CH_2Cl_2, scan rate: 50 mV/s, E vs Fc/Fc+.

View Article Online
DOI: 10.1039/D0CP00521E

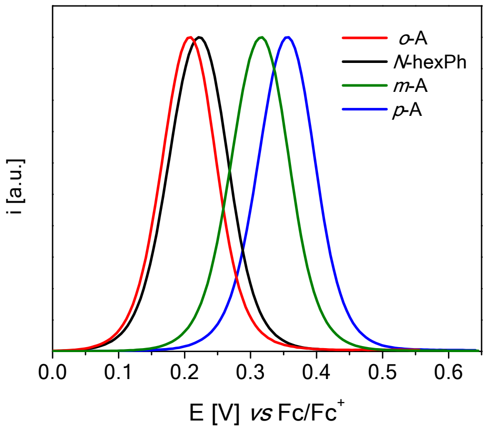

Fig. 2. Differential pulse voltammograms registered for oxidation of ***o*-A** (red line), ***m*-A** (green line), ***p*-A** (blue line) and *N*-hexylphenoxazine (*N*-hexPh) (black line). Electrolyte: 0.1 M Bu_4NBF_4/CH_2Cl_2, E *vs* Fc/Fc+. Modulation time: 50 ms, modulation amplitude: 10 mV, step potential: 5 mV.

Table 1. Oxidation and reduction potentials (*vs* Fc/Fc^+), ionization potential (IP) and electron affinities (EA) of acridone derivatives. IP and EA were calculated following a procedure reported in ref.[36], i.e. IP [eV] = |e|[1.15x $E_{ox\ onset}$ + 4.79] [eV], EA [eV] = e[1.18x$E_{redonset}$ + 4.83] [eV].

compound	E^0_{ox} [V]	E^0_{red} [V]	IP [eV]	EA [eV]	Eg
***o*-A**	0.212	-2.28	5.03	-2.14	2.89
***m*-A**	0.317	-2.23	5.15	-2.20	2.95
***p*-A**	0.360	-2.25	5.20	-2.18	3.02
di-*m*-A	0.332	-2.16	5.17	-2.28	2.89
N-hexylacridone	1.020	-2.44	5.96	-1.95	4.01
N-hexylphenoxazine	0.223	-	5.05	-	

Quantum chemical calculations

Four principal goals of the performed DFT studies were envisioned: i) elucidation of the molecules geometry; ii) determination of the shape and distribution of the frontier orbitals; iii) identification of dominant transitions and iv) theoretical calculations of IP and EA values. The calculated results are discussed in the perspective of the obtained experimental findings.

The donor and acceptor moieties of all derivatives are almost perpendicular to each other in both vacuum and a solution (see Figure S3 in *ESI*). Consequently, the HOMO and LUMO are located on different parts of the molecule. Spatial separation (small overlap) of the frontier orbitals inhibits the $S_0 \rightarrow S_1$ transition with a dominant HOMO→LUMO configuration (see Table 2). Thus, the lowest energy peak exhibiting high oscillator strength corresponds to a transition $S_0 \rightarrow S_n$, n>1, with a dominant configuration HOMO-1→LUMO. In the same way, if we consider the Kasha rule, small oscillator strength of the $S_1 \rightarrow S_0$ transition hinders the fluorescence *(vide infra)*. Therefore, emission in these molecules strongly depends on the change of the torsion angle between two conjugated moieties during the excited state relaxation.

Table 2. Excitation energies (*E*), wave lengths (λ), oscillator strengths (*f*), and dominant configurations of the three lowest excited states of the acridone derivatives calculated by means of the PCM-B3LYP-GD3BJ/6-311++G(d,p) method in toluene and dichloromethane.

Excited State	*E* [eV]	λ [nm]	*f*	Dominant configurations
Toluene				
***o*-A**				
S1	2.050	605	0.0013	HOMO→LUMO (99 %)
S2	3.176	390	0.0002	HOMO→LUMO+1 (97 %)
S3	3.350	370	0.1574	HOMO-1→LUMO (95 %)
***m*-A**				
S1	2.402	516	0.0001	HOMO→LUMO (99 %)
S2	3.370	368	0.0016	HOMO→LUMO+1 (96 %)
S3	3.373	368	0.1210	HOMO-1→LUMO (97 %)
***p*-A**				
S1	2.471	502	0.0029	HOMO→LUMO (98 %)
S2	3.351	370	0.1385	HOMO-1→LUMO (97 %)
S3	3.463	358	0.0026	HOMO→LUMO+1 (92 %)
Dichloromethane				
***o*-A**				
S1	2.177	569	0.0012	HOMO→LUMO (99 %)
S2	3.319	374	0.0309	HOMO→LUMO+1 (77 %) HOMO-1→LUMO (19 %)
S3	3.325	373	0.1268	HOMO-1→LUMO (78 %) HOMO→LUMO+1 (19 %)
***m*-A**				
S1	2.454	505	0.0001	HOMO→LUMO (99 %)
S2	3.343	371	0.1198	HOMO-1→LUMO (97 %)
S3	3.458	359	0.0014	HOMO→LUMO+1 (97 %)
***p*-A**				
S1	2.468	502	0.0032	HOMO→LUMO (98 %)
S2	3.322	373	0.1368	HOMO-1→LUMO (97 %)
S3	3.487	356	0.0018	HOMO→LUMO+1 (90 %)

Figure 3 shows the distribution of the frontier orbitals in ***o*-A**, ***m*-A** and ***p*-A** molecules. While HOMO is located on the phenoxazine moiety independently of the isomer, HOMO-1 and LUMO are found on the acridone one. This distribution strongly supports the electrochemical results implying that the

View Article Online
DOI: 10.1039/D0CP00521E

molecules are being oxidized at their phenoxazine parts and reduced at the acridone ones.

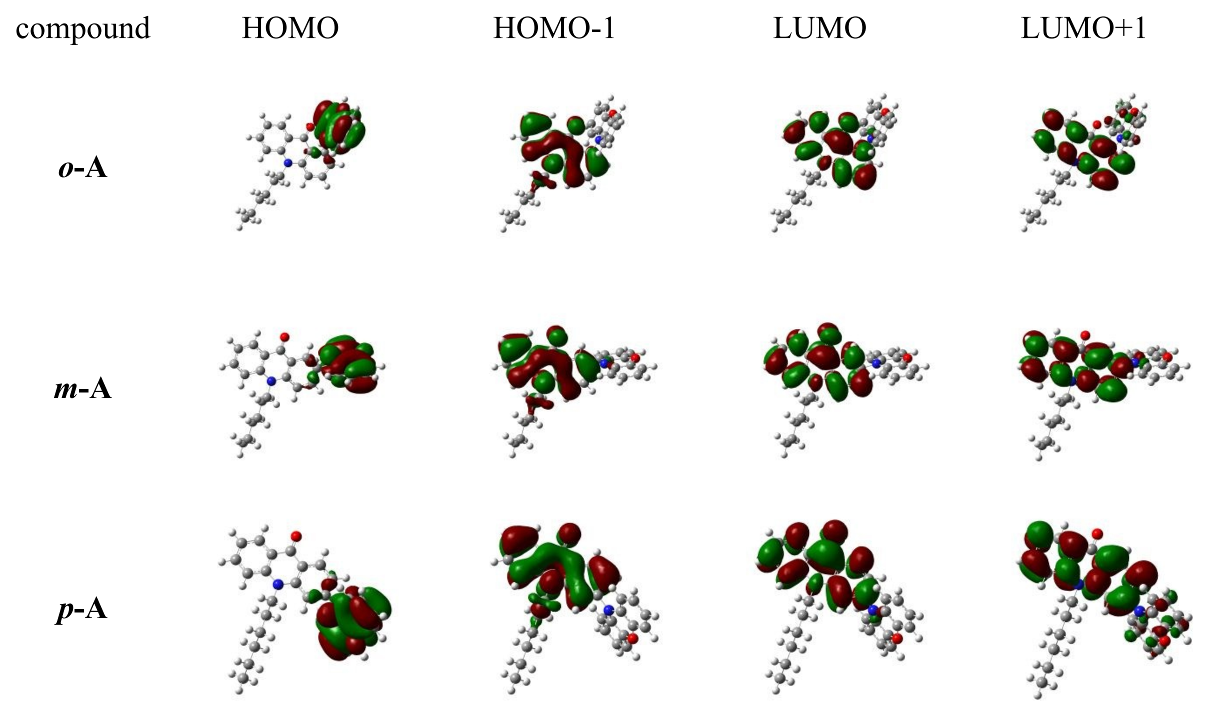

Fig. 3. HOMO, HOMO-1, LUMO, and LUMO+1 contours calculated using the PCM-B3LYP-GD3BJ/6-311++G(d,p) method in toluene

In Table 3 the results of the performed quantum chemical calculations of the electronic properties are collected. High consistency of the theoretical IP and EA values with the experimental ones should be pointed out. First, the calculated IPs were very close to the electrochemically determined ones, the latter being in between the values obtained using adiabatic and vertical approaches (compare data in Tables 1 and 3). Significantly weaker effect of the phenoxazine group position on the calculated EA values was also evidenced by DFT calculations, again consistent with the experimental findings, although the experiments gave |EA| values slightly lower than those obtained theoretically using the vertical approach.

Table 3. HOMO, LUMO, IP and EA values of ***o*-A**, ***m*-A** and ***p*-A** from DFT calculations carried out for vacuum and DCM*.

compound	conditions	HOMO	LUMO	E_g	$IP_{adiabatic}$	$IP_{vertical}$	$EA_{adiabatic}$	$EA_{vertical}$
***o*-A**	vacuum	4.72	-2.15	2.57	5.95	6.12	-0.95	-0.82
***o*-A**	DCM	5.08	-2.23	2.85	4.95	5.12	-2.35	-2.22
***m*-A**	vacuum	5.03	-2.17	2.86	6.24	6.45	-0.94	-0.82
***m*-A**	DCM	5.23	-2.25	2.98	5.08	5.26	-2.37	-2.24
***p*-A**	vacuum	5.16	-2.17	2.99	6.41	6.57	-0.96	-0.82
***p*-A**	DCM	5.27	-2.26	3.01	5.13	5.30	-2.40	-2.25

*All energies of HOMO, LUMO, ionization potential (IP), electron affinity (EA) given in eV and calculated by the method PCM-B3LYP-GD3BJ/6-311++G(d,p).

Easier oxidation (and by consequence lower IP) of ***o*-A** was not unequivocally reflected in its molecular geometry. We therefore analyzed the twist angle between the donor and acceptor parts of the molecule since this angle might determine the redox, electronic and optical properties of the studied molecules, as known for other D-A compounds.[37] In both vacuum and DCM the highest twist angles around the $C_{acridone}$-$N_{phenoxazine}$ was found for ***m*-A**, (*ca.* 89°), whereas for ***o*-A** and ***p*-A** the corresponding angles were between 78 and 84° (see Table 4 in the subsequent section where the calculated dihedral angles are compared with those obtained from X-ray studies).

Crystal structures

All three isomers readily form single crystals suitable for their structure determination. Detailed data collection as well as crystal structure refinement details are given in ESI (Table S2). *o*-A and *p*-A crystallize in $P\bar{1}$ and $P2_1/n$ space groups, respectively, with one molecule per asymmetric unit, while ***m*-A** crystallizes in the $P2_1/c$ space group with two molecules in

View Article Online
DOI: 10.1039/D0CP00521E

the asymmetric unit accompanied by disordered solvent molecules (see Figure 4 for their molecular structure).‡, § The inspection of the structure with the MP program reveals that the two ***m*-A** molecules are related by a pseudoinversion center located at 0.75, 0.12, 0.24 with the largest discrepancies exhibited by carbon atoms from aliphatic C_6H_{13}– substituents.[38] The interaction energy between the two molecules, estimated by the method of Spackman *et al.* [39,40] amounts to ca. −45 kJ/mol and results from carbonyl···carbonyl and C–H···π interactions (note that here and in the following the intermolecular interaction energy is the total energy of interaction between a pair of molecules and the designated interactions are the strongest contributors to the energy for the given pair of molecules, but they are not the only contributors). The strongest intermolecular interactions for both symmetry independent molecules occur between molecules interacting *via* C–H···O hydrogen bonds. These hydrogen bonds contribute mostly to the electrostatic term of the interaction energy. The total interaction energy is dominated by dispersion, though, occurring probably mainly between closely arranged hexyl chain and acridone moiety (see Table S3 for details). The crystal structure of ***p*-A** exhibits hierarchical supramolecular ordering. Molecules related by inversion center form dimers with the interaction energy of −56 kJ/mol. The dimers are in turn connected into double chains running along the crystallographic *Y* axis via C–H···π interactions with intermolecular interaction energy of −48 kJ/mol. The double layers in the crystallographic (001) planes are formed *via* C–H···O hydrogen bonds with an intermolecular interaction energy of −39 kJ/mol. The layers are linked into 3D structure mainly by dispersion interactions with no close contacts between the neighboring molecules (see Table S3-S5 for details of the intermolecular interactions). The intermolecular interaction energies in ***o*-A** are less varied than in the ***p*-A**, making the description of its crystal structure in terms of the supramolecular hierarchy impossible. The interactions in the crystal are dominated by π stacking and C–H···π interactions.

It is instructive to compare optimized geometries of neutral ***o*-A**, ***m*-A** and ***p*-A** molecules obtained on the basis of DFT calculations with their geometry in the solid state derived from XRD measurements. This comparison is presented in Table 4 where the values of the dihedral angle between the planes of acridone and phenoxazine are collected.

Table 4. Dihedral angles between donor and acceptor moieties of the neutral molecule determined by X-ray in the solid state and in the ground state calculated by the (PCM-B3LYP-GD3BJ/6-311++G(d,p) method (in degrees).

compound	X-ray	calculated		
		vacuum	DCM	toluene
***o*-A**	80.42(4)	82	83	83
***m*-A**	76.44(9), 79.83(10)	89	89	89
***p*-A**	78.20(4)	79	84	84

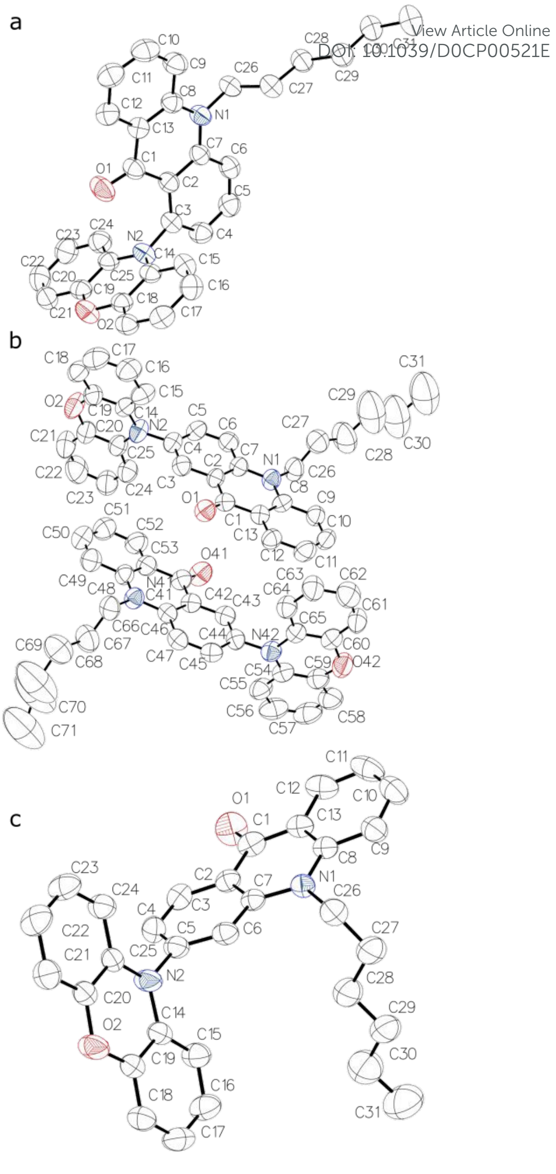

Fig. 4. Molecular structures of: a) ***o*-A**; b) ***m*-A** and c) ***p*-A** with atomic numbering scheme. Thermal ellipsoids drawn at the 50% probability level and hydrogen atoms omitted for clarity.

It could be noticed that the calculations of the geometry of an isolated molecule led to a conformation of the phenoxazine ring which was less planar than that determined in the solid state by X-ray diffraction. Also the conformation of the *n*-hexyl group of the *para* isomer was different in the crystal than that computed in vacuum by DFT. These conformational differences probably originate from the intermolecular interactions which promote a more efficient packing in the solid state.

View Article Online
DOI: 10.1039/D0CP00521E

Spectroscopic studies in solution

Acridone derivatives, in addition to reversible electrochemistry and ambipolarity, frequently exhibit interesting luminescent properties[22, 23]. For this reason we have undertaken detailed studies of the photophysics of ***o*-A**, ***m*-A** and ***p*-A**. Their absorption, fluorescence and phosphorescence in toluene (T) and dichloromethane (DCM) solutions were measured at room temperature and at 5 K. The absorption spectra of all three isomers showed two characteristic bands in the 375–425 nm spectral range (see Figure 5 and Table 5), which were essentially independent of the solvent. In the spectrum of o-A an additional broad absorption band with a clear maximum at 473 nm in T and at 460 nm in DCM (for the latter see Figure S4 in ESI) was present which could be attributed to a CT transition.

Table 5. Photophysical parameters derived from the spectroscopic measurements at RT of ***o*-A**, ***m*-A** and ***p*-A** at room temperature, where ϕ is the fluorescence quantum yield, τ the fluorescence decay time and k_r the radiative decay rate.

compound	solvent	$\lambda_{abs\ max}/\lambda_{fl\ max}$ [nm]	ϕ [%]	τ [ns]	k_r [10^7 s^{-1}]	Stokes shift [cm^{-1}]
***o*-A**	T	399,473 /618	1.37	15	0.091	4961
***o*-A**	DCM	403, 460/665	0.19	1.88	0.101	6701
***m*-A**	T	396/538	4.60	26	0.177	6665
***m*-A**	DCM	400/631	0.30	4.6	0.065	9152
***p*-A**	T	400/517	20	29	0.690	5657
***p*-A**	DCM	402/615	3.45	16	0.216	8616

The fluorescence spectra, registered at RT in both solvents, were broad and showed no vibrational structure. Contrary to the absorption spectra, they were solvent sensitive, showing the photoluminescence bands bathochromically shifted in DCM as compared to those registered in toluene. In the case of both solvents, the fluorescence quantum yields and fluorescence decay times increased in the inversed series: ***p*-A**> ***m*-A**> ***o*-A**, being however significantly higher for solutions in T as compared to DCM (see Table 5).

At 5 K prompt emission i.e. fluorescence was observed (Figure 6), exhibiting a decay time of some nanoseconds. It was accompanied by long-lived phosphorescence showing much longer decay times (see Figure 6 for the exact values). Both spectra nearly coincided and such observation could suggest that the singlet and the triplet states origin was of the charge-transfer character. It should be noted that the phosphorescence decay time determined for o-A was over two orders of magnitude shorter than in the case of m-A and p-A (2 ms vs 541 ms and 480 ms, respectively). Based on these observations it can be concluded that the CT character of the triplet state in ***o*-A** is higher than in the two other isomers, consistent with the absorption spectroscopy data.

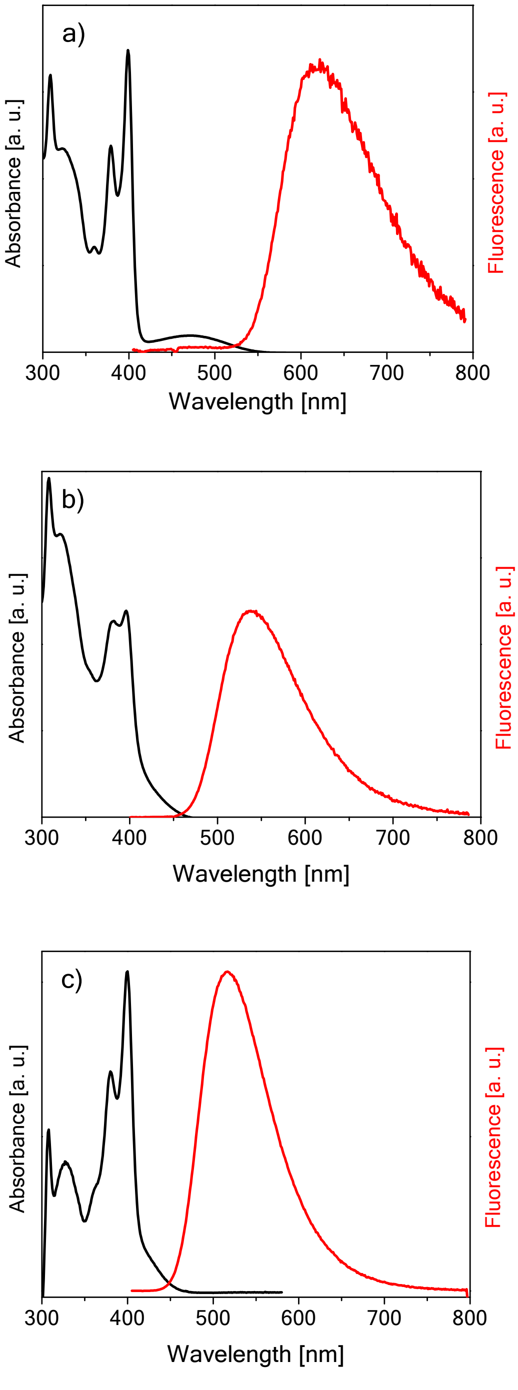

Fig. 5. Absorption and fluorescence spectra of ***o*-A** (a), ***m*-A** (b) and ***p*-A** (c) in toluene at RT, λ_{exc} = 400 nm.

The fluorescence to phosphorescence intensity ratio at 5 K was dependent on the solvent and varied for the studied isomers. The most intense phosphorescence at 5 K was observed for ***p*-A** in T. Therefore this sample was selected for the temperature dependence investigations in the temperature range inferior to the matrix melting point (178 K).

View Article Online
DOI: 10.1039/D0CP00521E

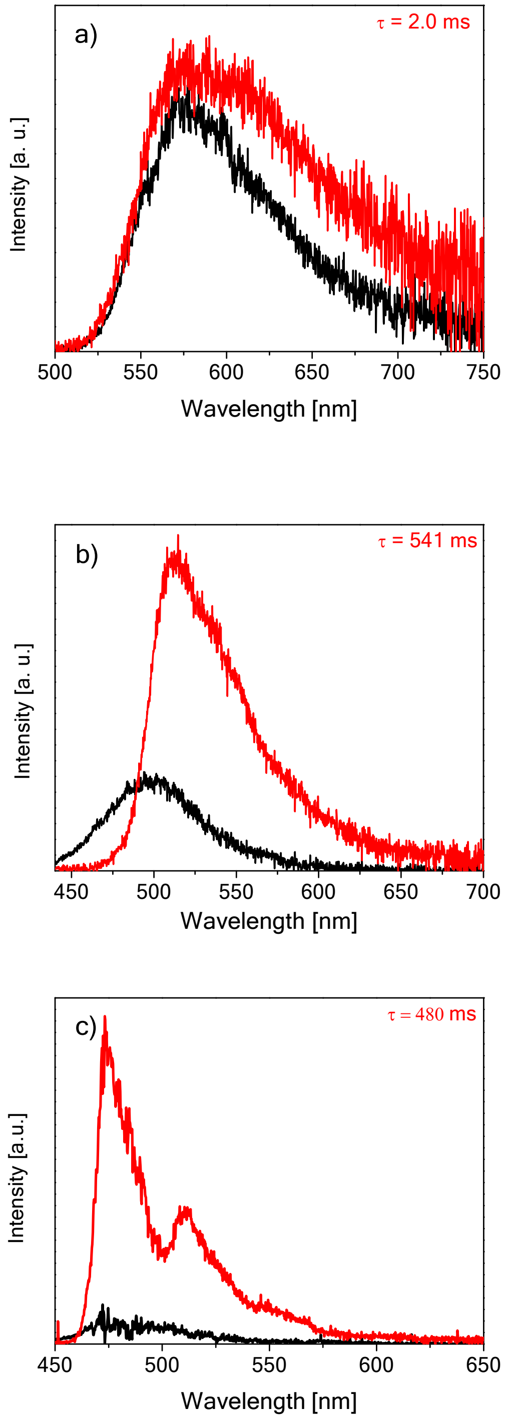

Fig. 6. Fluorescence (black) and phosphorescence (red) spectra of ***o*-A** (a), ***m*-A** (b) and ***p*-A** (c) in toluene at 5 K, λ_{exc} = 405 nm.

The phosphorescence intensity of ***p*-A** in toluene gradually decreased with the temperature raising from 12 to 150 K (Figure 7) and then it disappeared at 175 K (close to the toluene melting point). Its decay curves could be well fitted using a single exponential dependence, yielding decay times shortening from 516 to 461 ms upon the temperature raise from 12 to 75 K. At temperatures > 100 K decays of the long-lived emission became even shorter and clearly could not be expressed by a single exponential relationship. It showed a fast component contribution growing with temperature. Parallel to shortening of the long-lived emission decay, a decrease of this emission intensity could be observed together with a shift of the spectrum towards shorter wavelengths (see Figure 7). The prompt emission (in our phosphorimeter it composes of the emission which decays faster than 0.1 ms) intensity was approximately constant in the temperature range between 5 and 50 K, and started to increase at temperatures above 75 K. All these temporal observations of spectral changes seem to indicate that the thermal activation of delayed fluorescence is involved in these processes, which shortens the triplet state lifetime from millisecond to a microsecond time regime. In this case the detected prompt emission would be composed of fluorescence and delayed fluorescence.

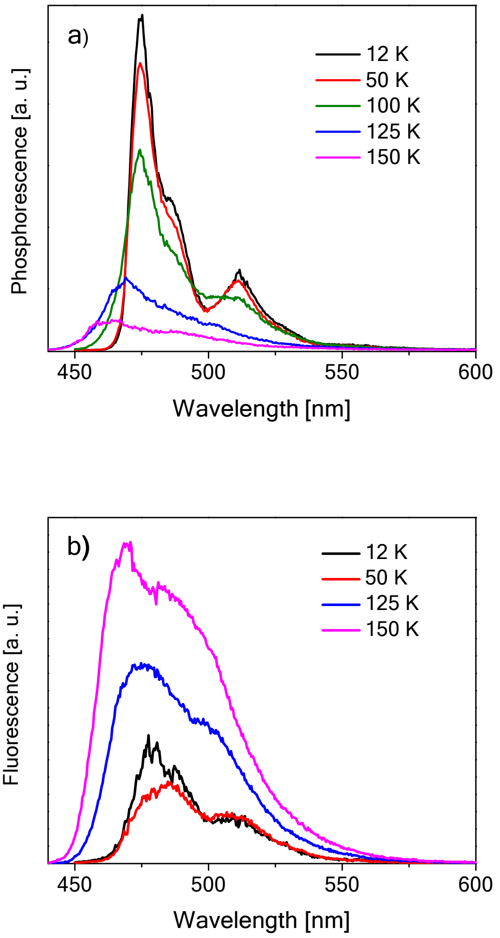

Fig. 7. Phosphorescence (a) and fluorescence (b) spectra of ***p*-A** in toluene at temperatures between 12 and 150 K.

Kinetic analysis of the triplet state thermal depopulation was however difficult in the case of the studies of ***p*-A** in toluene because of the presence of an ensemble of different ***p*-A** conformers, probably rotamers, frozen in the toluene matrix. Different rotamers could exhibit slightly different T_1-S_1 energy gaps, leading to non-exponential temporal activation. Thus, simple and convincing analysis of the thermally activated

View Article Online
DOI: 10.1039/D0CP00521E

delayed fluorescence (TADF), like that presented for a single crystal of the CT complex[10] , is not possible in the present case. At 175 K, *i.e.* close to the melting point of toluene, the long-lived emission disappeared and the prompt emission underwent a bathochromic shift of the spectrum maximum (from 470 to 537 nm). Such behavior can be considered as a manifestation of the strong dependence of the observed spectral features on the environment rigidity. These findings seems to be confirmed by the results obtained for the solid state emission of studied compounds (*vide infra*).

Modeling of thermally activated delayed fluorescence (TADF)

In order to model the TADF process, equilibrium geometries of relevant electronic states S_0, S_1, and T_1 were calculated by means of the COSMO-(TD)PBE0-GD3BJ/TZP method for all studied derivatives in toluene and dichloromethane. The obtained dihedral angles between donor and acceptor moieties are listed in Table 6. For the ground state, these dihedral angles are in a very good agreement with ones obtained at the PCM-B3LYP-GDBJ/6-311++G(d,p) level. For all S_0 and S_1 state geometries, the dihedral angles are within the range from 80° to 90°. On the other hand, dihedral angles determined for the T_1 geometry of the *meta*- and *para*-derivatives are significantly lower. While dihedral angles in the ground state are almost the same in both solvents, they are lower in dichloromethane for the excited state geometries.

Then, a SOC calculation was performed for all optimized structures by means of the COSMO-pSOC-TD PBE0-GD3BJ/TZP method. Properties of SOC excitations corresponding to the $S_1 \rightarrow S_0$ and $T_1 \rightarrow S_0$ transitions are summarized in Table 7. Oscillator strengths of the $T_1 \rightarrow S_0$ transitions are not shown, because they are negligible (less than 10^{-7}). It is obvious that also $S_1 \rightarrow S_0$ transitions at the S_1 geometries are very weak with oscillator strengths from 10^{-4} to 2×10^{-3}, that correspond to radiative lifetimes from 3×10^{-6} to 4×10^{-5} s. However, this transition is much stronger at the T_1 geometries of the *meta*- and *para*-derivatives with the oscillator strengths one to two order of magnitude greater (radiative lifetimes from 4×10^{-8} to 5×10^{-7} s) than at the S_1 geometry. Table 8 shows direct ($S_1 \rightarrow T_1$) and reverse ($T_1 \rightarrow S_1$) intersystem crossing rates k (for calculations see Eq. (1) in ESI) at RT along with the energy differences ΔE_{ST}, averaged SOC matrix elements $\left|\langle S_1 | \hat{H}_{SO} | T_1 \rangle\right|$ (see Eq. (5), ESI), and reorganization energies λ. Direct intersystem crossing rates in ***o*-A** are about one order of magnitude lower than in ***m*-A** and ***p*-A**. The reverse intersystem crossing rate in ***o*-A** dissolved in toluene is very low, while all other rates are in the range from 9×10^5 to 9×10^6 s^{-1}.

Table 6. Theoretical dihedral angles (in degrees) between the donor and acceptor moieties of the acridone derivative dissolved in dichloromethane and toluene. Calculation was performed by the COSMO-(TD)PBE0-GD3BJ/TZP method for the ground state (S_0) and lowest singlet (S_1) and triplet (T_1) excited states of the molecules.

Compound	DCM	Toluene
Ground state S_0		
***o*-A**	82	82
***m*-A**	88	88
***p*-A**	84	82
Excited state S_1		
***o*-A**	85	87
***m*-A**	87	90
***p*-A**	86	88
Excited state T_1		
***o*-A**	80	86
***m*-A**	61	66
***p*-A**	65	76

It should be pointed out that the values of the intersystem crossing rates strongly depend on the reorganization energies λ. Since computation of their external part λ_{ext} is complicated, some authors suggest using some empirical values, e.g. 0.1 eV, either for λ_{ext}, or for the whole λ, instead of its calculation according to Eq. (3) (see ESI).[41,42] Although incorporation of such empirical reorganization energies would alter the calculated intersystem crossing rates, it would not bring a new insight.

View Article Online
DOI: 10.1039/D0CP00521E

Table 7. Energies *E*, wave lengths λ, oscillator strengths *f*, and radiative lifetimes τ of the transitions from the lowest singlet (S_1) and triplet (T_1) excited states to the ground state in toluene and dichloromethane calculated at the S_1 or T_1 equilibrium geometry. Triplet oscillator strengths are not shown, because they are negligible.

Toluene solution

Derivative	Geometry	$E(S_1)$ [eV]	$\lambda(S_1)$ [nm]	$f(S_1)$	τ [s]	$E(T_1)$ [eV]	$\lambda(T_1)$ [nm]
***o*-A**	S_1	1.689	734	4.20E-04	1.93E-05	1.671	742
***o*-A**	T_1	1.688	735	4.76E-04	1.70E-05	1.667	744
***m*-A**	S_1	2.051	605	1.39E-04	3.93E-05	2.024	613
***m*-A**	T_1	2.152	576	9.82E-03	5.07E-07	2.020	614
***p*-A**	S_1	2.171	571	1.56E-04	3.13E-05	2.158	575
***p*-A**	T_1	2.206	562	3.36E-02	1.41E-07	2.161	574

Dichloromethane solution

Derivative	Geometry	$E(S_1)$ [eV]	$\lambda(S_1)$ [nm]	$f(S_1)$	τ [s]	$E(T_1)$ [eV]	$\lambda(T_1)$ [nm]
***o*-A**	S_1	1.838	675	7.54E-04	9.05E-06	1.818	682
***o*-A**	T_1	1.844	672	6.54E-03	1.04E-06	1.816	683
***m*-A**	S_1	2.109	588	7.24E-04	7.15E-06	2.077	597
***m*-A**	T_1	2.216	559	2.69E-02	1.75E-07	2.008	617
***p*-A**	S_1	2.164	573	1.84E-03	2.68E-06	2.150	577
***p*-A**	T_1	2.233	555	1.30E-01	3.55E-08	2.139	580

Table 8. Intersystem crossing rates *k*, calculated at room temperature, energy differences between singlet and triplet states ΔE_{ST}, and reorganization energies λ calculated for the direct ($S_1 \rightarrow T_1$) and reverse ($T_1 \rightarrow S_1$) intersystem crossing in toluene and dichloromethane solutions.

Toluene solution

Derivative	$k(S_1 \rightarrow T_1)$ [s^{-1}]	$k(T_1 \rightarrow S_1)$ [s^{-1}]	ΔE_{ST} [eV]	$\lvert\langle S_1 \lvert \hat{H}_{SO} \rvert T_1\rangle\rvert$ ($S_1 \rightarrow T_1$) [cm^{-1}]	$\lvert\langle S_1 \lvert \hat{H}_{SO} \rvert T_1\rangle\rvert$ ($T_1 \rightarrow S_1$) [cm^{-1}]	$\lambda(S_1 \rightarrow T_1)$ [eV]	$\lambda(T_1 \rightarrow S_1)$ [eV]
***o*-A**	2.3E+05	4.7E+03	0.020	0.015	0.021	0.002	0.001
***m*-A**	1.0E+06	9.2E+06	0.051	0.029	0.300	0.024	0.085
***p*-A**	8.5E+06	4.4E+06	0.019	0.058	0.083	0.007	0.033

Dichloromethane solution

Derivative	$k(S_1 \rightarrow T_1)$ [s^{-1}]	$k(T_1 \rightarrow S_1)$ [s^{-1}]	ΔE_{ST} [eV]	$\lvert\langle S_1 \lvert \hat{H}_{SO} \rvert T_1\rangle\rvert$ ($S_1 \rightarrow T_1$) [cm^{-1}]	$\lvert\langle S_1 \lvert \hat{H}_{SO} \rvert T_1\rangle\rvert$ ($T_1 \rightarrow S_1$) [cm^{-1}]	$\lambda(S_1 \rightarrow T_1)$ [eV]	$\lambda(T_1 \rightarrow S_1)$ [eV]
***o*-A**	2.1E+05	2.2E+06	0.021	0.020	0.047	0.001	0.011
***m*-A**	6.0E+06	1.3E+06	0.106	0.085	0.344	0.074	0.120
***p*-A**	5.5E+06	9.2E+05	0.041	0.061	0.082	0.027	0.088

On the basis of these results, we can describe the excited state relaxation in the following way. Excitation to an absorbing state S_n, n>1, is followed by the internal conversion to S_1 state according to the Kasha rule. Oscillator strengths $f(S_1)$ of the $S_1 \rightarrow S_0$ transition, calculated at S_1 geometry, are small due to almost perpendicular mutual position of the donor and the acceptor moieties (see Table 6). Thus, prompt emission in all derivatives should be very small. However, it should be pointed out that the potential energy surface of the S_1 state is rather flat in the vicinity of the S_1 equilibrium geometry. Therefore, the dihedral angle between the donor and acceptor moieties can thermally fluctuate within a certain range *ca.* from 75° to 105°, which induces an increase in the oscillator strengths $f(S_1)$. Consequently, values of the measured fluorescence radiative decay rates k_r (see Table 5) are considerably greater than those corresponding to the oscillator strengths $f(S_1)$ calculated at the equilibrium geometry (see Table 7). Nevertheless, fluorescence is relatively weak, which is a necessary condition for the direct intersystem crossing $S_1 \rightarrow T_1$. Although SOC matrix elements are rather small, this process is facilitated by its exothermic character. While there may be a significant competition between the prompt emission and the intersystem crossing in the *ortho*-derivative, the latter should be favored in others.

For ***o-A***, dihedral angles between donor and acceptor moieties remain close to 90° also during relaxation of the T_1 state, especially in toluene. Thus, also SOC matrix element remains relatively small. Consequently, our model does not expect reverse intersystem crossing $T_1 \rightarrow S_1$ in the *ortho*-derivative in toluene. Although it should be possible in dichloromethane, TADF is in this case limited by a very small oscillator strength. Simultaneously, probability of

View Article Online
DOI: 10.1039/D0CP00521E

Therefore, some kind of phosphorescence $T_1 \rightarrow S_0$ was found to be negligible. non-radiative deexcitation should prevail in the case of this monomer.

For ***m*-A** and ***p*-A**, the dihedral angle between the donor and acceptor planes significantly decreases during the T_1 state relaxation. This molecular deformation leads to an increase of the SOC matrix elements, and consequently also the reverse intersystem crossing rates, namely in the *meta*-derivative. On the other hand, relaxation of the T_1 state is also accompanied an increase of the energy difference ΔE_{ST} and the reorganization energies λ, which have the opposite effect. Consequently, the reverse intersystem crossing rates in dichloromethane are lower than in toluene. Another consequence of the reduced dihedral angle is greater overlap between HOMO and LUMO, which promotes $S_1 \rightarrow S_0$ emission, but oscillator strengths of the $T_1 \rightarrow S_0$ phosphorescence remains negligible. Therefore, fluorescence may occur, but only before subsequent relaxation of the molecular conformation to the S_1 equilibrium geometry. If the molecule is not deexcited, it may undergo repeated direct and reverse intersystem crossing transitions.

We are aware of the fact that there exists a dynamic competition between emission and non-radiative decay processes, which were not included in our model. However, we can assume that the non-radiative decay in all isomers may occur with comparable rates due to their similar chemical structure. Then, considering the radiative lifetimes shown in Table 7 and intersystem crossing rates in Table 8, we can expect more efficient TADF in ***m*-A** and ***p*-A** as compared to ***o*-A**. Nevertheless, it should be remarked that our model considers only molecules in their lowest-energy equilibrium conformations, instead of a Boltzmann distribution of conformations present in real solvents. Some non-equilibrium conformations of ***o*-A** in the T_1 state may possess significantly lower dihedral angles between the donor and acceptor moieties than the equilibrium conformation. For such molecules, values of the intersystem crossing rates and oscillator strength of the $S_1 \rightarrow S_0$ emission may be comparable with values obtained for ***m*-A** and ***p*-A.** Consequently, our model cannot exclude possibility of an efficient TADF also in ***o*-A.**

Spectroscopic studies in the solid state

If applications of the studied new derivatives are to be considered, spectroscopic properties of their thin films have to be determined. Drop casting and spin coating techniques were used for the preparation of thin solid layers of pure ***o*-A**, ***m*-A** and ***p*-A** yielding films of comparable quality. Additionally, samples of these derivatives molecularly dispersed in a solid matrix (2 wt% and 5.5 wt% of a given compound in zeonex) were fabricated by spin coating. Zeonex is a convenient matrix for dispersing luminophores since the resulting films are usually uniform and show excellent optical quality.

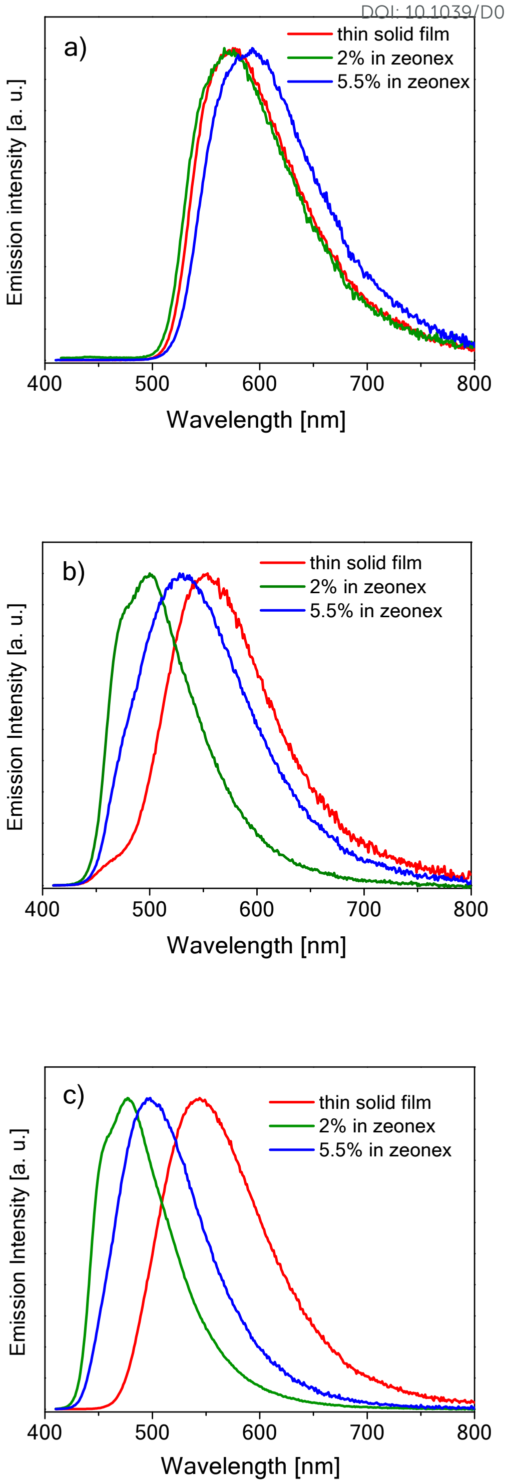

Fig. 8. Emission spectra of solid thin film of pure compounds and their dispersions in zeonex (2 wt % and 5.5 wt%): a) ***o*-A** b) ***m*-A** and c) ***p*-A**.

View Article Online
DOI: 10.1039/D0CP00521E

Table 9. Photophysical parameters derived from the spectroscopic measurements of ***o*-A**, ***m*-A** and ***p*-A** at room temperature, where ϕ is the fluorescence quantum yield.

compound	composition	$\lambda_{abs\ max}/\lambda_{fl\ max}$ [nm]	ϕ [%]
***o*-A**	2% in zeonex	396,480/575	13
	5.5% in zeonex	397,477/590	9.5
	thin solid film	366,407/575	13
***m*-A**	2% in zeonex	393,550/500	10
	5.5% in zeonex	393,565/530	10
	thin solid film	389,411/555	4
***p*-A**	2% in zeonex	393/477	30
	5.5% in zeonex	397/497	33
	thin solid film	310,367,406/545	16

Absorption spectra of the studied molecules dispersed in zeonex closely resemble the corresponding solution (T or DCM) spectra. The positions of the dominant peak in the spectra of all isomers are similar. However, they are slightly hypsochromically shifted: by 3 nm for ***o*-A,** 4 nm for ***m*-A** and 7 nm for ***p*-A** with respect to the corresponding peaks registered for solutions in T (compare data collected in Tables 5 and Table 9) To the contrary, in the spectra of thin films of pure compounds, bathochromic shifts are observed as compared to those recorded in T by 8 nm (***o*-A**), 15 nm (***m*-A**) and 6 nm (***p*-A**).

The emission spectra of thin solid films of pure compounds are more sensitive to isomerism (see Figs. 8 a, b. and c). The wavelength of the emission band peak decreases in the following order: ***o*-A**> ***m*-A**> ***p*-A**. In the case of ***m*-A** and ***p*-A** the emission bands are substantially bathochromically shifted with respect to the peaks recorded in T which can indicate strong intermolecular interactions, less significant in ***o*-** isomer where a hypsochromic shift is observed. All solid state emission spectra are hypsochromically shifted with respect to the corresponding solution spectra recorded in DCM.

In the case of molecules dispersed in zeonex hypsochromic shifts, with respect to the corresponding bands in the solution spectra (T and DCM), are observed for all compounds studied (compare Tables 5 and 9). These observations coincide very well with fluorescence temperature dependence measurements and confirm the sensitivity of molecules emission to the rigidity of the environment which makes relaxation of emissive states difficult.

Significantly higher ϕ values were measured for thin films of pure compounds and films of these compounds dispersed in zeonex, as compared to ϕ values measured for solutions. The most pronounced increase of ϕ was observed for ***o*-A** where it reached 13% both for pure ***o*-A** films and for 2 wt% dispersion of this isomer in zeonex, whereas in the case of its solution spectra (T) the values of ϕ were one order of magnitude lower. Similar phenomenon was reported for a phenoxazine derivative of xanthen-9-on, a somehow similar compound to those described here. It was rationalized by suppression of different vibration-induced emission quenching mechanisms, existing in solution but nonexistent in the solid state due to intermolecular interactions confinements.[43]

Conclusions

To summarize, we have synthesized three positional isomers of phenoxazine-substituted acridone, namely of 1-phenoxazine-*N*-hexylacridone (***o*-A)**, 2-phenoxazine-*N*-hexylacridone (***m*-A)** and 3-phenoxazine-*N*-hexylacridone (***p*-A).** The investigated compounds show very interesting electrochemistry. In particular, their electrochemical oxidation, occurring on phenoxazine moiety at relatively low potentials is reversible and isomerism-sensitive. The reduction of the acridone moiety is irreversible, little dependent on isomerism and starts at rather low potentials. The values of ionization potentials (IP) and electron affinities (EA) calculated from the electrochemical data are in a very good agreement with those predicted by DFT calculations.

Stationary and time-resolved spectroscopic investigations carried in toluene at different temperatures in all three cases revealed features indicating a significant contribution of thermally activated delayed fluorescence (TADF) to the observed emission.

A theoretical model of the TADF process in studied compounds was proposed based on quantum chemical calculations. It suggests an important role of the conformation relaxation in the T_1 state, namely decrease of the dihedral angle between donor and acceptor moieties to the values around 70°, which enables both the reverse intersystem crossing $T_1 \rightarrow S_1$ and subsequent $S_1 \rightarrow S_0$ emission. These values of the dihedral angle are in a very good agreement with ones recently proposed by Weissenseel et al. for an efficient TADF in 4,4′-(10*H*,10′*H*-9,9′-spirobi[acridine]-10,10′-diyl)-dibenzonitrile (SBABz4).[44]

Finally, the determined photoluminescence quantum yields (ϕ) were systematically higher for solid state films of pure compounds and for their dispersions in solid matrices (zeonex) as compared to the ϕ values measured for solutions. The effect was rationalized by suppression of different vibration-induced emission quenching mechanisms taking place in solutions and nonexistent in the solid state due to intermolecular interactions confinements.

Conflicts of interest

There are no conflicts to declare.

Acknowledgement

This work was supported by the National Science Centre, Poland (NCN, Grant No. 2015/17/B/ST5/00179). M.B. and B.K. additionally acknowledge financial support from National Science Centre, Poland under QuantERA programme, project no 2017/25/Z/ST2/03038. P.A.G. thanks Warsaw University of Technology for financial support. P.T. acknowledges financial support from the Czech Science Foundation, grant No. 17-02578S. The access to computing and storage facilities owned by parties and projects contributing to the National Grid Infrastructure MetaCentrum provided under the programme "Projects of Large Research, Development, and Innovations Infrastructures" (CESNET LM2015042), and to the Wroclaw

Centre for Networking and Supercomputing (WCSS) is gratefully acknowledged.

Notes and references

‡ Molecular formula and formula weight for ***o*-A, *m*-A** and ***p*-A:** $C_{31}H_{28}N_2O_2$ (M =460.55 g/mol). **Crystal Data** for ***o*-A**: triclinic, space group $P\overline{1}$ (no. 2), a = 9.3283(7) Å, b = 10.2674(8) Å, c = 13.0289(9) Å, α = 79.338(6)°, β = 87.728(6)°, γ = 73.749(7)°, V = 1177.24(16) Å^3, Z = 2, T = 293(2) K, 16699 reflections measured, 4629 unique (R_{int} = 0.0380). The final R_1 was 0.0512 ($I > 2\sigma(I)$) and wR_2 was 0.1545 (all data). **Crystal Data** for ***m*-A**: monoclinic, space group $P2_1/c$ (no. 14), a = 12.0942(9) Å, b = 14.5020(9) Å, c = 28.554(2) Å, β = 90.589(7)°, V = 5007.8(6) Å^3, Z = 8, T = 293(2) K, 52508 reflections measured, 9828 unique (R_{int} = 0.0958). The final R_1 was 0.0883 ($I > 2\sigma(I)$) and wR_2 was 0.3318 (all data). **Crystal Data** for ***p*-A**: monoclinic, space group $P2_1/n$ (no. 14), a = 7.9995(3) Å, b = 14.2069(6) Å, c = 21.3942(9) Å, β = 100.552(4)°, V = 2390.29(17) Å^3, Z = 4, T = 293(2) K, 25561 reflections measured, 4692 unique (R_{int} = 0.0327). The final R_1 was 0.0494 ($I > 2\sigma(I)$) and wR_2 was 0.1452 (all data).

§CCDC 1949980-1949982 contain supplementary crystallographic data for this paper. These data can be obtained free of charge from The Cambridge Crystallographic Data Centre via https://www.ccdc.cam.ac.uk/structures/.

1 B.G. Kim, X. Ma, C. Chen, Y. Ie, E.W. Coir, H. Hashemi, Y. Aso, P.F. Gree, J. Kieffer, J. Kim, *Adv. Funct. Mater.*, 2013, **23**, 439.
2 A. Casey, S.D. Dimitrov, P. Shakya-Tuladhar, Z. Fei, M. Nguyen, Y. Han, T.D. Anthopoulos, J.R. Durrant, M. Heeney, *Chem. Mater.*, 2016, **28**, 5110.
3 M.Y. Wong, E.Zysman-Colman, *Adv. Mater.*, 2017, **29**, 1605444 (1-54).
4 P. Bujak, I. Kulszewicz-Bajer, M. Zagorska, V. Maurel, I. Wielgus, A. Pron, *Chem. Soc. Rev.*, 2013, **42**, 8895.
5 Y. Lin, X. Zhan, *Acc. Chem. Res.*, 2016, **49**, 175.
6 C. Zhan, J. Yao, *Chem. Mater.*, 2016, **28**, 1948.
7 J. Zhang, J. Jin, H. Xu, Q. Zhang, W. Huang, *J. Mater. Chem. C*, 2018*,* **6**, 3485.
8 L. Bieniek, B.C. Schroeder, C.B. Nielsen, I. McCulloch, *J. Mater. Chem.*, 2012*,* **22**, 14803.
9 A. Pron, R. R. Reghu, R. Rybakiewicz, H. Cybulski, D. Djurado, J. V. Grazulevicius, M. Zagorska, I. Kulszewicz-Bajer, J.-M. Verilhac, *J. Phys. Chem. C* 2011, **15**, 15008.
10 B. Kozankiewicz, J. Prochorow, *Mol. Cryst. Liq. Cryst.* 1987, **148**, 93.
11 H. Kaji, H. Suzuki, T. Fukushima, K. Shizu, K. Suzuki, S. Kubo, T. Komino, H. Oiwa, F. Suzuki, A. Wakamiya, Y. Murata, C. Adachi, *Nat. Commun.*, 2015, **6**, 8476.
12 M.K. Etherington, F. Franchello, J. Gibson, T. Northey, J. Santos, J.S. Ward, H.F. Higginbotham, P. Data, A. Kurowska, P. Lays Dos Santos, D.R. Graves, A.S. Batsanov, F.B. Dias, R. Bryce, T.J. Penfold, A.P. Monkman, *Nat. Commun.*, 2017, **8**, 14987.
13 T. Jarosz, K. Gebka, A. Stolarczyk, W. Domagala, *Polymers*, 2019, **11**, 273.
14 X. Lv, W. Li, M. Ouyang, Y. Zhang, D.S. Wright, C. Zhang, *J. Mater. Chem. C*, 2017, **5**, 12.
15 P.M. DiCarmine, T.B. Schon, T.M. McCormick, P.P. Klein, D.S. Seferos, *J. Phys. Chem. C*, 2014, **118**, 8295.
16 Y. Guo, W. Li, H. Yu, D.F. Perepichka, H. Meng, *Adv. Energ. Mater.*, 2017, **7**, 1601623.
17 J. Zapala, M. Knor, T. Jaroch, A. Maranda-Niedbala, E. Kurach, K. Kotwica, R. Nowakowski, D. Djurado, J. Pecaut, M. Zagorska, A. Pron, *Langmuir*, 2013, **29**, 14503.
18 J. Zhang, W. Chen, S. Kalytchuk, K.F. Li, R. Chen, C. Adachi, Z. Chen, A.L. Rogach, G. Zhu, P.K.N. Yu, W. Zhang, K.W. Cheah, X. Zhang, C.S. Lee, *ACS Appl. Mater. Interfaces*, 2016, **8**, 11355.
19 D.A.K. Vezzu, J.C. Deaton, M. Shayeghi, Y. Li, S. Huo, *Org. Lett.*, 2009, **11**, 4310.
20 Q.T. Siddiqui, A.A. Awasthi, P. Bhui, M. Muneer, K.R.S. Chandrakumar, S. Bose, N. Agarwal, *J. Phys. Chem. C*, 2019, **123**, 1003.
21 K.D. Theriault, C. Radford, M. Pavez, B. Heyne, T.C. Sutherland, *Phys. Chem. Chem. Phys.*, 2015, **17**, 20903.
22 B.K. Sharma, A.M. Shaikh, N. Agaewal, R.M. Kamble, *RSC Adv.*, 2016, **6**, 17129.
23 P. Pander, A. Swist, R. Motyka, J. Soloducho, F.B. Dias, P. Data, *J. Mater. Chem. C*, 2018, **6**, 5434.
24 C. Lee, W. Yang, R.G. Parr, *Phys. Rev. B,* 1988, **37,** 785.
25 A.D. Becke, *J. Chem. Phys.,* 1993, **98,** 5648.
26 S. Grimme, S. Ehrlich, L. Goerigk, *J. Comput. Chem.,* 2011, **32,** 1456.
27 E. Makrlík, P. Toman, P. Vaňura, *Monatsh. Chem.,* 2014, **145**, 551.
28 S. Ehala, P. Toman, R. Rathore, E. Makrlík, V. Kašička, *Electrophoresis,* 2011, **32**, 981.
29 S. Záliš, I. Kratochvílová, A. Zambová, J. Mbindyo, T.E. Mallouk, T.S. Mayer, *Eur. Phys. J. E,* 2005, **18,** 201.
30 J. Tomasi, B. Mennucci, R. Cammi, *Chem. Rev.,* 2005, **105,** 2999.
31 R. Bauernschmitt, R. Ahlrichs, *Chem. Phys. Lett.,* 1996, **256,** 454.
32 M. E. Casida, C. Jamorski, K. C. Casida, D. R. Salahub, *J. Chem. Phys.,* 1998, **108,** 4439.
33 R. E. Stratmann, G. E. Scuseria, M. J. Frisch, *J. Chem. Phys.,* 1998, **109,** 8218.
34 M. J. Frisch, G. W. Trucks, H. B. Schlegel, G. E. Scuseria, M. A. Robb, J. R. Cheeseman, G. Scalmani, V. Barone, G. A. Petersson, H. Nakatsuji, X. Li, M. Caricato, A. V. Marenich, J. Bloino, B. G. Janesko, R. Gomperts, B. Mennucci, H. P. Hratchian, J. V. Ortiz, A. F. Izmaylov, J. L. Sonnenberg, D. Williams-Young, F. Ding, F. Lipparini, F. Egidi, J. Goings, B. Peng, A. Petrone, T. Henderson, D. Ranasinghe, V. G. Zakrzewski, J. Gao, N. Rega, G. Zheng, W. Liang, M. Hada, M. Ehara, K. Toyota, R. Fukuda, J. Hasegawa, M. Ishida, T. Nakajima, Y. Honda, O. Kitao, H. Nakai, T. Vreven, K. Throssell, J. A. Montgomery, Jr., J. E. Peralta, F. Ogliaro, M. J. Bearpark, J. J. Heyd, E. N. Brothers, K. N. Kudin, V. N. Staroverov, T. A. Keith, R. Kobayashi, J. Normand,K. Raghavachari, A. P. Rendell, J. C. Burant, S. S. Iyengar, J. Tomasi, M. Cossi, J. M. Millam, M. Klene, C. Adamo, R. Cammi, J. W. Ochterski, R. L. Martin, K. Morokuma, O. Farkas, J. B. Foresman, and D. J. Fox, Computer program Gaussian 16, Revision B.01, Gaussian, Inc., Wallingford CT, 2016.
35 C. Wolf, S. Liu, X. Mei, A.T. August, M.D. Casimir, *J. Org. Chem.,* 2006, **71**, 3270.
36 J. Sworakowski, J. Lipiński, K. Janus, *Org. Electronics*, 2016, **33**, 300.
37 R.S. Nobuyasu, J.S. Ward, J. Gibson, B.A. Laidlaw, Z. Ren, P. Data, A.S. Batsanov, T.J. Penfold, M.R. Bryce, F.B. Dias, *J. Mater. Chem. C*, 2019, **7**, 6672.
38 R. A. Baggio, *Acta Cryst. C,* 2019, ***75* (7)**, 837.

View Article Online
DOI: 10.1039/D0CP00521E

View Article Online
DOI: 10.1039/D0CP00521E

39 M.J. Turner, S. Grabowsky, D. Jayatilaka, M.A. Spackman, *J. Phys. Chem. Lett.* 2014, **5 (24)**, 4249.

40 C.F. Mackenzie, P.R. Spackman, D. Jayatilaka, M.A. Spackman,. *IUCrJ,* 2017, **4 (5)**, 575.

41 P.K. Samanta, D. Kim, V. Coropceanu, J.-L. Brédas, *J. Am. Chem. Soc.,* 2017, **139,** 4042.

42 S. Xu, Q. Yang, Y. Wan, R. Chen, S. Wang, Y. Si, B. Yang, D. Liu, C. Zheng, W. Huang, *J. Mater. Chem. C,* 2019, **7,** 9523.

43 Y. Zhang, H. Ma, S. Wang, Z. Li, K. Ye, J. Zhang, Y. Liu, Q. Peng, Y. Wang, *J. Phys. Chem. C* 2016, **120**, 19759.

44 S. Weissenseel, N.A. Drigo, L.G. Kudriashova, M. Schmid, T. Morgenstern, K.-H. Lin, A. Prlj, C. Corminboeuf, A. Sperlich, W. Brütting, M. K. Nazeeruddin, V. Dyakonov: *J. Phys. Chem. C,* 2019, **123,** 27778.

TOC

View Article Online
DOI: 10.1039/D0CP00521E

Electrochemical and fluorescent (TADF) properties of phenoxazine derivatives of acridone are strongly isomerism-sensitive.

View Article Online
DOI: 10.1039/D0CP00521E